


## Defect theory under steady illuminations and applications

Guo-Jun Zhu , Yi-Bin Fang, Zhi-Guo Tao, Ji-Hui Yang,\* and Xin-Gao Gong

Key Laboratory for Computational Physical Sciences (MOE), State Key Laboratory of Surface Physics,

Department of Physics, Fudan University, Shanghai 200433, China

and Shanghai Qizhi Institution, Shanghai 200232, China

 (Received 29 March 2023; revised 9 July 2023; accepted 8 September 2023; published 17 October 2023)

Illumination has been long known to affect semiconductor defect properties during either growth or operating processes. Current theories of studying the illumination effects on defects usually have the assumption of unaffected formation energies of neutral defects as well as defect transition energy levels, and use the quasi-Fermi levels to describe behaviors of excess carriers with conclusions at variance. In this work, we first propose a method to simulate steady illumination conditions, based on which we demonstrate that formation energies of neutral defects and defect transition energy levels are insensitive to illumination. Then, we show that optical and thermal excitation of electrons can be seen equivalent with each other to reach a steady electron distribution in a homogeneous semiconductor. Consequently, the electron distribution can be characterized using just one effective temperature  $T'$  and one universal Fermi level  $E'_F$  for a homogeneous semiconductor under continuous and steady illuminations, which can be seen as a combination of quasiequilibrium electron system with  $T'$  and a lattice system with  $T$ . Using these concepts, we uncover the universal mechanisms of illumination effects on charged defects by treating the band-edge states explicitly on the same footing as the defect states. We find that the formation energies of band-edge “defect” states shift with increased  $T'$  of electrons, thus affecting the  $E'_F$ , changing defect ionic probabilities, and affecting concentrations of charged defects. We apply our theory to study the illumination effects on the doping behaviors in GaN:Mg and CdTe:Sb, obtaining results in accordance with experimental observations. More interesting experimental defect-related phenomena under steady illuminations are expected to be understood from our theory.

DOI: [10.1103/PhysRevResearch.5.043049](https://doi.org/10.1103/PhysRevResearch.5.043049)

### I. INTRODUCTION

Defects play central roles in determining various properties of semiconductors [1–4]. However, defect characterizations are very challenging experimentally. Thanks to the development of defect theories, especially the first-principles defect calculations, semiconductor devices and applications have been greatly advanced in the past decades [5–7]. Nevertheless, present theoretical defect studies mainly focus on semiconductors under equilibrium conditions without considering practical operations. Recently, illumination was reported to influence the device performance and material properties for photocatalytic and photovoltaic semiconductors by affecting defect behaviors during either operating or growth processes [8–12]. The underlying mechanisms, however, remain elusive. Defect theories under illuminations are therefore necessary to further promote the development of semiconductor techniques.

Among various defect-related properties, defect formation energy and transition energy level are the two most crucial quantities: the former determines the defect concentration, and the latter, defined as the energy cost to get ionized, determines the ability of a defect to provide carriers. How illumination plays roles in affecting these two quantities is hence the first problem to be solved. Several theoretical schemes have been proposed so far to study the illumination effects on defect formations by: (1) assuming illuminations do not change the formation energies of neutral defects and defect transition energy levels; and (2) using the quasi-Fermi levels (QFLs) to define formation energies of charged defects [9,13–17]. These schemes are unsatisfactory, nonetheless, because the former assumption is not justified due to lack of efficient calculation methods to simulate the illumination conditions for defect supercells, while the latter has the problem of defining QFLs when various defects, excess electrons and holes are present together under illuminations. In fact, different works using different definitions yield different results. For example, Alberi defined a QFL for each kind of defect and reported that the concentration of dominate defects increased while the concentration of compensational defects decreased under illumination [14]. In contrast, Cai *et al.* assumed two quasi-Fermi reservoirs and proposed a weight to define different QFLs for donors, acceptors, and free carriers. They found that all charged defects tend to have the increased formation energies under illumination for any semiconductor [9]. In addition,

\*jhyang04@fudan.edu.cn

Published by the American Physical Society under the terms of the [Creative Commons Attribution 4.0 International license](https://creativecommons.org/licenses/by/4.0/). Further distribution of this work must maintain attribution to the author(s) and the published article's title, journal citation, and DOI.

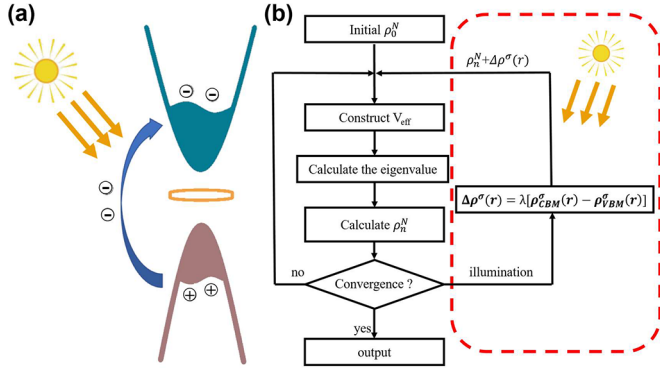


FIG. 1. Simulation method of steady illumination. (a) Diagram shows electron excitations and occupations under illuminations. (b) Sketching flow chart for self-consistent calculations under steady illuminations.

the definitions of defect QFLs in some works rely on the carrier capture and emission rates, which are often difficult to be obtained accurately both theoretically and experimentally [9,14,15]. To understand defect behaviors under illuminations, defect calculation methods considering illumination conditions are eagerly awaited to be developed, and universal defect theories under illuminations should be established thereafter.

In this work, we first propose a method to simulate continuous and steady illumination conditions, based on which we demonstrate that formation energies of neutral defects and defect transition energy levels are insensitive to illumination. Then, we show that optical and thermal excitation of electrons can be approximately seen as equivalent with each other to reach a steady electron distribution. Consequently, the electron distribution can be characterized using just one effective temperature  $T'$  and one universal Fermi level  $E'_F$ . And, a semiconductor under continuous and steady illuminations can be seen as a combination of quasiequilibrium electron system with temperature  $T'$  and an equilibrium lattice system with temperature  $T$ . Under illuminations, by treating the band-edge states explicitly on the same footing as the defect states, the formation energies of band-edge defect states shift with increased  $T'$  of electrons, thus affecting the  $E'_F$  of the electron system, changing the ionic probabilities of defect states, and affecting concentrations of charged defects. We apply the present theory to study the illumination effects on the doping behaviors in GaN:Mg and CdTe:Sb and obtain consistent results with experimental observations. We expect that more interesting experimental defect-related phenomena under steady illuminations can be understood from our theory.

## II. ILLUMINATION EFFECTS ON NEUTRAL DEFECT

Under defect dilute approximations, illuminations mainly excite electrons from the valence bands to the conduction bands. With the help of phonons, the photogenerated electrons (holes) will soon be relaxed to the band edges and the whole system will reach a steady state, as shown in Fig. 1(a). To simulate excess carriers under continuous and steady illuminations, previous works often adopted a method of electron-occupation constraining scheme, i.e., by reducing the occupation number at the valance-band maximum (VBM)

state and increasing the occupation number at the conduction-band minimum (CBM) state simultaneously [18]. However, when a defect is created in a semiconductor supercell, one cannot find the exact VBM or CBM states anymore due to band couplings [19,20].

To simulate defects under illuminations, here an alternative way is adopted to simulate excess carriers by constraining charge densities instead of electron occupations. As we know, illuminations change the electron occupations and thus the total charge-density distributions. Therefore, if the correct charge-density distributions are adopted under illuminations, according to the density functional theory the correct total energy of a defective supercell can be obtained, which we mainly concern in defect calculations. To mimic the steady state under illuminations, we add a charge-density correction, i.e.,  $\Delta\rho^\sigma(r) = \lambda[\rho_{\text{CBM}}^\sigma(r) - \rho_{\text{VBM}}^\sigma(r)]$  [Here,  $\lambda$  is the number of excited electrons from the VBM to the CBM and can be used to represent the illumination intensity.  $\rho_{\text{CBM}}^\sigma(r)$  and  $\rho_{\text{VBM}}^\sigma(r)$  are the partial charge density of the spin-polarized CBM and VBM states, respectively], to the total charge density without illuminations. Note that for simulations of semiconductors without any defects, the charge-correction method is exactly equivalent to the electron-occupation constraining scheme. However, for defective supercells, our method is physically more meaningful by using real band-edge charge density [19]. We implement the charge-correction method in the QUANTUM ESPRESSO code [21] and the flow chart is shown in Fig. 1(b). The  $\Delta\rho$  is applied in each electronic step during the self-consistent process to make sure the total charge density can always give a physically meaningful description of the illumination conditions.

Now we can calculate the formation energies of neutral defects under illuminations according to the definition, which is

$$\Delta H_f^{il}(\alpha, q) = E^{il}(\alpha, q) - E^{il}(\text{host}) + \sum n_i(\mu_i + E(i)) + q(E_F + \varepsilon_{\text{VBM}}) + \Delta^q, \quad (1)$$

where  $E^{il}(\alpha, q)$  and  $E^{il}(\text{host})$  are the total energies of the supercell under illuminations with a defect  $\alpha$  charged  $q$  and without any defects, respectively.  $E(i)$  refers to the total energy of the element  $i$  in its pure stable phase,  $\mu_i$  is the chemical potential of element  $i$  referenced to  $E(i)$ , and  $n_i$  is the number of  $i$  atoms removed from (positive) or put in (negative) the supercell in the process of defect formation.  $\Delta^q$  includes all necessary terms such as core-level alignments, finite-size corrections [22–24], and low-dimensional corrections [25]. We take the Madelung energy of an array of point charges with neutralizing background and the alignment of the VBM as the corrections [24]. The defect-transition energy levels under illuminations  $E_i^{\alpha, il}(0/q)$  can also be calculated as

$$\begin{aligned} E_i^{\alpha, il}(0/q) &= [E^{il}(\alpha, q) - E^{il}(\alpha, 0)]/(-q) + \varepsilon_{\text{VBM}}, (q < 0), \\ E_i^{\alpha, il}(0/q) &= \varepsilon_{\text{CBM}} - [E^{il}(\alpha, q) - E^{il}(\alpha, 0)]/(-q), (q > 0), \end{aligned} \quad (2)$$

where  $\varepsilon_{\text{VBM}}$  and  $\varepsilon_{\text{CBM}}$  are the energy levels of the CBM and VBM states, respectively. Other defect properties under steady illuminations such as defect-diffusion barriers and

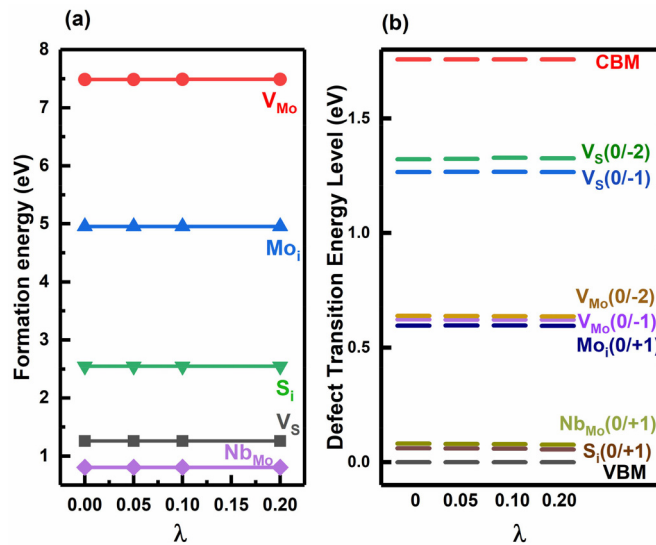


FIG. 2. Illumination effects on formation energies of neutral defects and defect-transition energy levels in MoS<sub>2</sub> monolayer. (a) Formation energies of neutral defects and (b) defect-transition energy levels as functions of illumination intensities.  $\lambda$  represents number of excited electrons at band edges in supercell, and defect-transition levels are referenced to VBM without illumination.

defect-assisted nonradiative recombination can also be processed in this scheme.

The charge-correction method is applied to study defect properties of MoS<sub>2</sub> monolayer and bulk, which is a representative system to show how illuminations affect defect properties in two-dimensional and three-dimensional materials (see Appendix A for details about charge-correction method). As an important semiconductor that has been studied abundantly, the defects in MoS<sub>2</sub> are essential in determining electrical [26,27], magnetic [28], and optical properties [29,30]. Our calculated formation energies of selected neutral defects in monolayer MoS<sub>2</sub> (see Appendix C for defects in bulk MoS<sub>2</sub>) including both intrinsic defects  $V_S$ ,  $V_{Mo}$ ,  $Mo_i$ ,  $S_i$ , and the impurity  $Nb_{Mo}$  as functions of illumination intensities are shown in Fig. 2(a) and the corresponding defect-transition energy levels are given in Fig. 2(b). Here, the illumination intensities are corresponding to an excess carrier density of 0 and  $6.4 \times 10^{12} \text{ cm}^{-2}$  for  $\lambda = 0$  and 0.2, respectively. Our results without illuminations agree well with previous works (see the discussion in Appendix C) [31,32]. With the increase of illumination intensities, we find that the formation energies of neutral defects and defect-transition energy levels have little changes. As shown in Fig. 2, the change of formation energy is less than 1 meV and that of defect-transition energy level is less than 0.1 meV. Such phenomena can be attributed to the delocalization of band-edge states, which have negligible effects on localized properties such as formation and ionization of an isolated defect. Our results demonstrate that illumination effects on formation energies of neutral defects and defect-transition energy levels can be reasonably discarded, but other defect properties such as diffusion barriers should be dealt with carefully. In the following, we will not distinguish formation

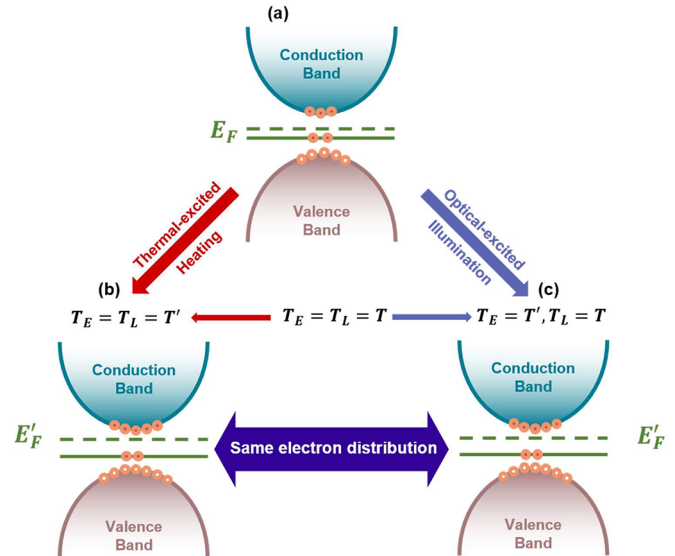


FIG. 3. Diagrams show thermal and optical excitation processes of electrons in semiconductor. (a) Band diagram shows electron distributions in equilibrium semiconductor system with defects under no illuminations. Note that electrons have same temperature as lattice and universal Fermi level of  $E_F$ . (b) Band diagram shows electron distributions after reaching equilibrium state due to temperature increase from  $T$  to  $T'$ . Now, system has universal Fermi level of  $E'_F$ . (c) Band diagram shows electron distributions after reaching steady state under continuous illuminations. Note that electron distributions in (b) and (c) are equivalent.  $T_E$  means effective electron temperature;  $T_L$  means lattice temperature.

energies of neutral defects and defect-transition energy levels with or without illuminations unless otherwise stated.

### III. ILLUMINATION EFFECTS ON CHARGED DEFECT

Different from formation of neutral defects which is only related to crystal lattices and little affected by illuminations, formation of charged defects relied on electron potentials, that is, the Fermi reservoirs. How to define the Fermi level or QFLs under illuminations has been a key challenge in this field. We start to think of this problem from the excitation of electrons in a semiconductor with some defect  $\alpha$  dilute and homogeneously distributed, which is initially at a thermal equilibrium state with a lattice temperature of  $T$ , a Fermi level of  $E_F$ , and a free-electron (-hole) density of  $n_0$  ( $p_0$ ) [see Fig. 3(a)]. We keep the total amount of defects fixed to focus solely on the electron behaviors at this stage as we will show the electron and lattice systems can be dealt with separately. We consider thermal excitations first. When the temperature is increased to  $T'$ , more carriers are generated from thermal excitations of both band and defect states. In the meanwhile, carriers are recombined via band-to-band transitions or via defect levels. When the generation rate is equal to the recombination rate, i.e.,

$$G = R_{BB} + R_{Aug} + \sum_{\alpha, q} R_{SRH}(\alpha, q), \quad (3)$$

where  $R_{BB}$ ,  $R_{Aug}$ , and  $R_{SRH}(\alpha, q)$  are the band-to-band, Auger, and defect-assisted Shockley-Read-Hall recombination rates,

respectively, electrons reach a steady distribution, that is, concentrations of free carriers, ratio of neutral and charged defects do not change anymore, as shown in Fig. 3(b). In this case, electrons reach an equilibrium state when the electron potentials in the conduction bands ( $E_{Fc}$ ), valence bands ( $E_{Fv}$ ), and defect states ( $E_{FD}$ ) are the same, i.e., electrons in the whole system share the same Fermi level  $E_F$ . From statistical physics, the electron potentials are defined according to

$$n' = N_C(T') \exp\left(-\frac{E_C - E_{Fc}}{k_B T'}\right), \quad (4)$$

$$p' = N_V(T') \exp\left(-\frac{E_{Fv} - E_V}{k_B T'}\right), \quad (5)$$

$$N(\alpha, q) = N(\alpha, 0) \exp\left(\frac{q * (E_t^\alpha - E_{FD})}{k_B T'}\right), \quad (6)$$

$$E_{Fc} = E_{Fv} = E_{FD} = E'_F. \quad (7)$$

Here,  $N_C(T')$  and  $N_V(T')$  are the effective density of states for the conduction band and the valence band at  $T'$ , respectively.  $E_C$  and  $E_V$  are the energy level of the CBM and VBM, respectively.  $k_B$  is the Boltzmann constant,  $N(\alpha, q)$  and  $N(\alpha, 0)$  are the concentrations of charged and neutral defects, respectively.  $E_{Fc}$ ,  $E_{Fv}$ , and  $E_{FD}$  are the Fermi level of electrons at the conduction bands, valence bands, and defect states, respectively.

Now, we consider optical excitation [see Fig. 3(c)]. Instead of increasing temperature to  $T'$ , we apply illumination to excite electrons in the system while keeping the lattice temperature  $T$  unchanged (the heating effect of illumination on lattices is neglected due to, i.e., dissipations to the environment). The optically excited hot electrons (holes) will soon relax to the CBM (VBM), forming a steady electron distribution. In principle, the same or similar electron distribution as in the case of Fig. 3(b) can be achieved by applying proper illuminations. This is reasonable because the behaviors of hot carriers after thermal or optical excitations are similar and one cannot distinguish thermal from optical excitations by just considering electron distributions. Because the two electron distributions are approximately equivalent, we can say that the electrons in Fig. 3(c) have an effective temperature of  $T'$  and a Fermi level of  $E'_F$ , especially if  $T'$  does not differ too much from  $T$  so that we can reasonably use  $N_V(T')$  and  $N_C(T')$  to approximate the real  $N_V$  ( $N_C$ ). Under the experimental conditions, this criterion is often satisfied. Take GaN as an example, as seen in the following discussions; the value of  $T'$  is about 1800 K compared to the growth temperature  $T$  of 1275 K under a power density of  $\sim 1$  W/cm<sup>2</sup> illumination. Note that the different temperatures for electrons and lattices in Fig. 3(c) indicate that the system is not a fully equilibrium system. Instead, it can be regarded as a combination of a quasiequilibrium electron system and an equilibrium lattice system.

From above discussions, we learn that thermal excitation of electrons is equivalent to optical excitation. Both thermal excitations and illuminations can “heat” electrons while the heating effect of illuminations on lattice is negligible due to the heat dissipations to the environment, especially when the environment temperature is high. Consequently, when a homogeneous semiconductor under continuous illuminations reaches a steady state with a certain distribution of electrons,

we can define an effective temperature  $T'$  and an effective Fermi level  $E'_F$  according to Eqs. (4)–(7) to characterize the electron distributions. In practice,  $T'$  can be self-consistently determined through Eqs. (3)–(7), given carrier generation rate due to illumination intensities as well as carrier recombination rates. Alternatively,  $T'$  can also be known according to Eqs. (4) and (5) if total carriers  $n'$  and  $p'$  are known. Meanwhile, a real temperature  $T$  should be used to define properties unrelated to the Fermi reservoir, i.e., the equilibrium concentration of neutral defects under illuminations should be still determined according to

$$N^{il}(\alpha, 0) = N(\alpha, 0) = gN_{\text{site}}(\alpha) \exp\left(\frac{-\Delta H_f(\alpha, 0)}{k_B T}\right), \quad (8)$$

where  $N_{\text{site}}(\alpha)$  is the number of possible sites of defect  $\alpha$  in a supercell,  $T$  is the real lattice temperature, and  $g$  is the degeneracy factor of the electron occupations. For charged defects under illuminations, the equilibrium concentration should be determined according to Eq. (6) as it is related to the Fermi reservoir. In addition, the overall charge-neutrality relation remains, that is,

$$\sum_{\alpha, q} q * N^{il}(\alpha, q) + p' - n' = 0. \quad (9)$$

By self-consistently solving Eqs. (3)–(9), we can obtain defect concentrations, carrier densities, and the effective Fermi level in a semiconductor at a given illumination intensity (i.e., given generation rate  $G$ ,  $T'$  or  $n'p'$ ).

Now we turn to study the illumination effects on formation of charged defects. Without loss of generality, we consider two kinds of defects ( $A$  and  $B$ ) and assume they are all at their ionized states ( $A^+$  and  $B^-$ ) with transition-energy levels of  $E_t^A$  and  $E_t^B$ . In real systems, defects could be vacancies, interstitials, antisites, or even complexes and have various charged states. Nevertheless, our analysis holds for any case. Figures 4(a)–4(c) show defect formation energies as functions of Fermi levels following conventional diagrams in defect calculations. It is noteworthy that as both formation energies of neutral defects and defect transition energy levels do not change with illumination intensities, the formation energy lines for charged defects [the solid lines,  $\Delta H_f^{il}(A^+) = \Delta H_f^{il}(A^0) - q * (E_t^A - E'_F)$ ,  $\Delta H_f^{il}(B^-) = \Delta H_f^{il}(B^0) - q * (E_t^B - E'_F)$ ] do not change under illuminations either. Because illuminations mainly play roles through affecting the band-edge excitations, we should treat the band-edge states explicitly on the same footing as the defect states. As we did in Ref. [33], the electron occupation at the conduction band under illuminations [see Eq. (4)] can be treated as having a singly charged “acceptor” with its formation energy of  $\Delta H_f^{il}(n') = k_B T' \ln\left[\frac{gN_{\text{site}}}{N_C(T')}\right] + E_g - E'_F$  and a transition energy level at the VBM. Similarly, hole occupation in the valence band under illuminations [see Eq. (5)] can be treated as an effective, singly ionized “donor” with its formation energy of  $\Delta H_f^{il}(p') = k_B T' \ln\left[\frac{gN_{\text{site}}}{N_V(T')}\right] + E'_F$  and a transition-energy level at the CBM. The formation energies of band-edge defects are shown in dashed lines in Figs. 4(a)–4(c).

Without illuminations, i.e.,  $T' = T$ , the entanglements between defects and band-edge excitations have been discussed

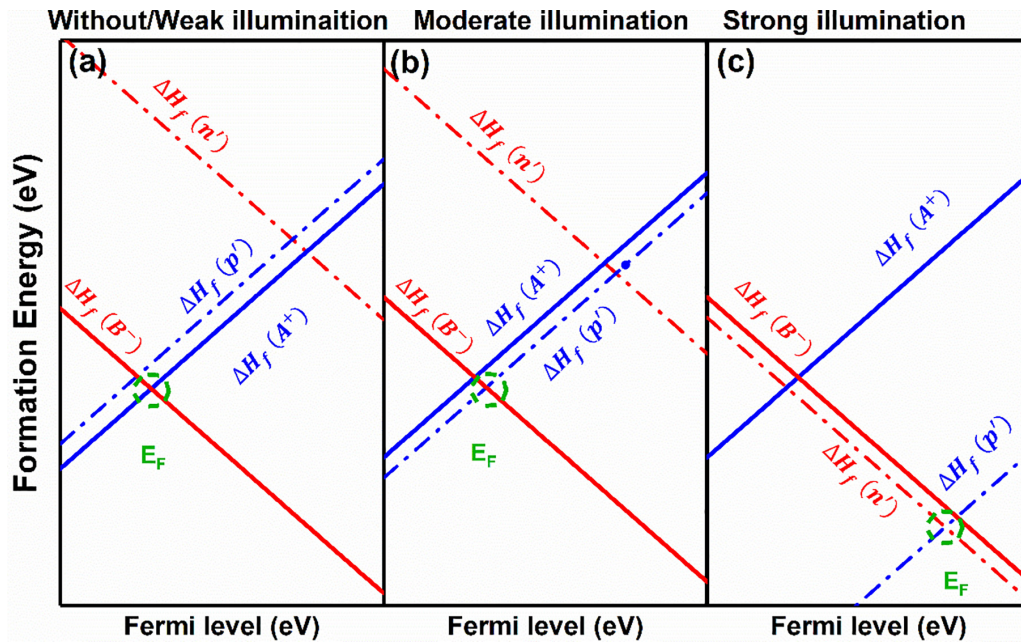


FIG. 4. Diagrams show formation energies of defects and band-edge defect functions of Fermi level under different illumination conditions. (a)–(c) Defect-formation energies under no (weak), moderate, and strong illuminations, respectively. Solid lines are for defects and dashed lines are for band-edge excitations.

in our previous work [33]. Here as an example, we just discuss the case of defect excitation dominant over thermal excitation under no illuminations, that is, the dashed lines are both above the solid lines in Fig. 4(a). Other cases can be analyzed in a similar way. With the applied of illuminations,  $T'$  increases and so do  $N_V(T')$  and  $N_C(T')$ . Usually, the dashed lines for  $\Delta H_f^{il}(n')$  and  $\Delta H_f^{il}(p')$  will shift upwards [due to  $N_V(T'), N_C(T') > gN_{\text{site}}$ ] and then shift downwards. Under weak illumination, the dashed lines are still above the solid lines. Consequently, the Fermi level has little changes as the  $E'_F$  is always mainly determined by defects. However, due to the increase of  $T'$ , the ratio between charged and neutral defects will decrease according to Eq. (6). As the concentration of neutral defects does not change under illumination, the concentration of charged defects will decrease for both dominant and compensated defects.

When the illumination intensities are increased to make the band-edge excitations comparable with defect excitations, i.e.,  $\Delta H_f^{il}(n')$  line is lower than  $\Delta H_f^{il}(B^-)$  and/or  $\Delta H_f^{il}(p')$  line is lower than  $\Delta H_f^{il}(A^+)$  as seen in Fig. 4(b), the  $E'_F$  will be determined by both band-edge and defect excitations. In this case, the  $E'_F$  can move to the middle of the band gap or to the band edges, depending on practical situations, and the change of the concentration of charged defects has no definite direction but has to be determined according to Eq. (9) (more detailed discussions are presented in Appendix D). When the illumination intensity is further increased so that the defect excitation is not important compared to band-edge excitations [see Fig. 4(c)], the  $E'_F$  is just determined by the  $N_V$  and  $N_C$ . An interesting phenomenon is that when  $N_V$  is larger than  $N_C$ , no matter whether the semiconductor is  $n$  type or  $p$  type initially, it will always turn into  $n$  type under extremely strong

illuminations. Similarly, when  $N_C$  is larger than  $N_V$ , the semiconductor will always be  $p$  type under extremely strong illuminations.

#### IV. ILLUMINATION EFFECTS ON GaN:Mg

We now apply our defect theory under illuminations to study illumination effects on defect properties of GaN during the growth process. It is reported that  $V_N$  is the main compensating center for the acceptor  $\text{Mg}_{\text{Ga}}$  in GaN under the Ga-rich condition [34,35]. Many works of literature have reported that illumination can increase the hole concentration but the mechanisms are not clear [36–38].

By using the first-principles defect calculations (see the calculation details in Appendix F), we obtain that  $\text{Mg}_{\text{Ga}}$  has a  $(0/-)$  transition-energy level around 0.25 eV above the VBM, while  $(+ / 0)$  and  $(3+ / 0)$  transition-energy levels of  $V_N$  locate at about 3.30 and 0.42 eV above the VBM, respectively, which are in good agreement with previous works [9,39]. The calculated defect-formation energies as functions of the Fermi level under the Ga-rich condition are shown in Fig. 5(a). The lines for band-edge defects are also given at  $T = 1275$  K, which is a typical experimental growth temperature. To obtain  $N_C$  and  $N_V$ , the electron and hole effective masses of  $0.2m_0$  and  $1.5m_0$  are used [40], respectively. When illumination is applied, the effective temperature of electrons starts to increase from  $T$  to  $T'$ . Note that given illumination intensities and thus  $T'$ , defect concentrations, carrier densities, and the  $E'_F$  can be obtained by self-consistently solving Eqs. (4)–(9) at a given growth temperature. In the following, we use  $\Delta n = n' - n_0$  to denote illumination intensities, where  $n'$  and  $n_0$  are the electron densities at electron temperatures of  $T'$  and  $T$  (here  $T = 1275$

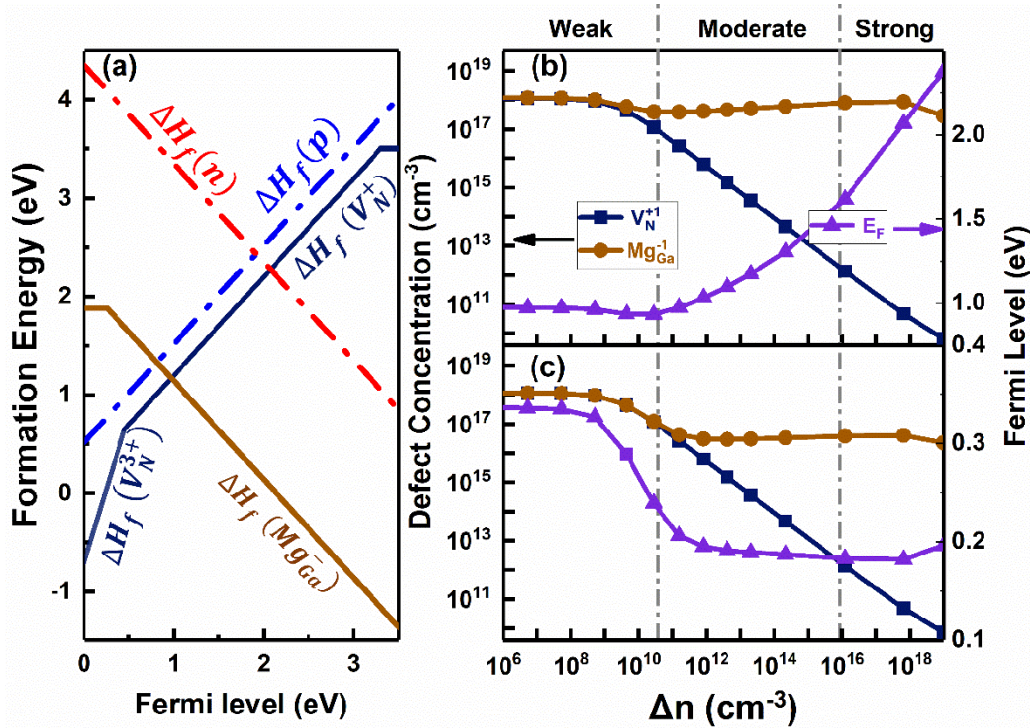


FIG. 5. Illumination effects on defect properties of Mg-doped GaN. (a) Defect-formation energies as functions of Fermi level in Mg-doped GaN. (b) Concentrations of charged defects and effective Fermi level as functions of illumination intensities when GaN is grown at 1275 K. (c) Concentrations of charged defects and Fermi levels after samples in (b) are quenched to 300 K and illuminations are removed.

K), respectively. In fact, we can also use  $T'$  to represent the illumination intensity and the results are consistent with each other (see Appendix F). Our calculated results of the illumination effects on charged defects in GaN are shown in Fig. 5(b). As can be seen,  $Mg_{Ga}^-$  and  $V_N^+$  behave very differently under illuminations, which can be explained as follows based on our theory.

First, without illumination, because the defect excitation is dominant over the band-edge excitations, the Fermi-level position will be pinned around the cross point of the formation-energy lines of  $Mg_{Ga}^-$  and  $V_N^+$ , which is about 1.0 eV above the VBM, making the GaN:Mg system a  $p$ -type semiconductor with the concentration of holes much larger than that of electrons. When illumination is applied, the dashed lines in Fig. 5(a) will shift down. Depending on the illumination intensities, there are three situations according to Fig. 4. Under weak illuminations when defect excitation is always much stronger than band-edge excitations, the concentration of photoexcited carriers contributes little to total free carriers and the Fermi-level position will be still pinned around the cross point of the formation-energy lines of  $Mg_{Ga}^-$  and  $V_N^+$  (as shown in Fig. 5(a)). Consequently, the  $E_F'$  does not change and the concentrations of all the charged defects will decrease because of the increased  $T'$  according to our above analysis in Fig. 4(a). Indeed, our results in Fig. 5(b) confirm our picture, i.e., both the concentrations of domination defects  $Mg_{Ga}^-$  and the compensation defects  $V_N^+$  decrease until  $\Delta n = 10^{11} cm^{-3}$ . With increased illumination and when  $\Delta n > 10^{11} cm^{-3}$  corresponding to the moderate illumination condition, the band-edge excitation starts to be comparable to or even dominate over the excitation of  $V_N^+$ . In this case,

the concentration of free electrons, which is now mainly contributed by photoexcited electrons, increases much more rapidly than that of free holes contributed by both  $Mg_{Ga}^-$  and photoexcited holes. Consequently, the  $E_F'$  would be shifted towards the middle of the band gap. Together with the increased  $T'$ , the increase of the Fermi level leads to the decrease of the concentration of  $V_N^+$  and the increase of the concentration of  $Mg_{Ga}^-$  according to Eq. (6). That is why  $Mg_{Ga}^-$  and  $V_N^+$  behave differently in this region. Note that the illumination intensity under experimental growth conditions [41,42] corresponding to  $\Delta n$  being about  $10^{12} - 10^{14} cm^{-3}$  lies just in this region. The first decrease under weak illumination and then increase under moderate illumination of the concentration of  $Mg_{Ga}^-$  lead to the nearly unchanged concentration of  $Mg_{Ga}^-$  coincidentally. In contrast, the decrease of the concentration of  $V_N^+$  under both weak and moderate illumination results in the significantly reduced amount of  $V_N^+$ . We find that the experiments only reported suppressed formation of  $V_N$  but no change of Mg-doping concentration [41,42], which is in good agreement with our results. When the illumination further increases, i.e.,  $\Delta n > 10^{16} cm^{-3}$  (suppose this can be achieved), the band-edge excitations will surpass defect excitations [see Fig. 5(b), Fig. 9(c)]. In this region, GaN will become more intrinsic and the  $E_F'$  will start to be closer to the CBM, turning GaN from  $p$  type to  $n$  type due to the smaller  $N_C$  compared to the  $N_V$ . In addition, the concentration of  $V_N^+$  continues to decrease due to the decreased  $q * (E_i^\alpha - E_F')$  and increased  $k_B T'$  in Eq. (6), while the  $Mg_{Ga}^-$  starts to decrease because the  $q * (E_i^\alpha - E_F')$  increases slower than  $k_B T'$ .

Illumination effects on charged defects offers a way for manipulating defect formation during the growth process. For

practical application, a sample is grown at a high temperature with appropriate illumination applied during the growth or postgrowth process until a quasiequilibrium status of electrons is achieved. Then, the illumination is removed and the sample is quenched to room temperature, assuming defects are fixed and only electrons are redistributed [43]. Our simulation results for GaN are shown in Fig. 5(c). As we can see, compared to the samples grown without illumination, the samples grown with illumination can have significantly shallower Fermi level close to the VBM after quenching and removal of illumination, making a large amount of  $\text{Mg}_{\text{Ga}}^-$  transform to  $\text{Mg}_{\text{Ga}}^0$  to balance the reduced amount of  $V_{\text{N}}^+$ . As a result, the concentration of hole increases from  $5 \times 10^{19}$  to  $28 \times 10^{19} \text{cm}^{-3}$  which is consistent with the experimentally reported increases from  $8.4 \times 10^{19}$  to  $22 \times 10^{19} \text{cm}^{-3}$  before and after illumination [41].

We also apply our theory to the Sb doping in CdTe and reasonably good agreement with available experiments is achieved. Especially, our theory can successfully explain the solubility increase of Sb doping due to illuminations during growth (see Appendix G), which cannot be understood from previous theories. In addition to manipulating defect properties during the growth process, illumination during operations at room temperature can also have significant effects by enhancing band excitations, changing the ratio between charged and neutral defects and shifting the  $E'_F$ . We expect our theory to provide both quantitative and qualitative explanations for many interesting experimental phenomena under steady illuminations.

## V. CONCLUSION

In summary, we have proposed a self-consistent method to simulate the continuous and steady illumination conditions. We have proved that the illumination effects on formation energies of neutral defect and defect-transition energy levels are negligible. To characterize electron distributions in a homogeneous semiconductor under continuous and steady illuminations, we have pointed out that thermal excitations are equivalent to optical excitations for reaching a steady electron distribution. Therefore, the electron distribution can be characterized by using just one effective temperature  $T'$  and one universal Fermi level  $E'_F$ . Based on the above concepts, we have uncovered the mechanisms of the illumination effects on defects by treating the band-edge states explicitly on the same footing as the defect states. We have found that the formation energies of band-edge defect states shift with increased  $T'$  of electrons, thus affecting the  $E'_F$  of the total system, changing the ionic probabilities of defect states, and affecting concentrations of charged defects. Our proposed picture falls in line with the experimental observations and has been exemplified by GaN:Mg and CdTe:Sb systems. More experimental works are strongly called for to test our defect theory under illuminations.

## ACKNOWLEDGMENTS

This work was supported in part by National Natural Science Foundation of China (Grant No. 12188101), the Special Funds for Major State Basic Research (Grant No.

2022YFA1404603), National Natural Science Foundation of China (Grants No. 11991061 and No. 11974078). Computations were performed at the High-Performance Computing Center of Fudan University.

## APPENDIX A: REVISED CHARGE-CORRECTION METHOD

Before the illumination, the valence bands are fully occupied by electrons and the conduction bands (CB) are empty at  $T = 0$ . Apparently, the whole system is a ground state and the total energy denoted as  $E$  can be easily obtained from the ground-state calculations. With the illumination, the electrons in the valence band are excited to the conduction band. Under thermodynamic equilibrium condition, the electron (hole) will finally be relaxed to CBM (VBM) state. We present the diagrams to show the excitation process under continuous and steady illumination in Fig. 1(a) in the main text. Since the timescale for the hot electron (hole) to relax to the CBM (VBM) is much shorter than that for excess carriers to recombine between the CBM and VBM either radiatively or nonradiatively, we can use the change of the band-edge charge density to describe the steady state under illumination conditions. Accordingly, the total charge density has a change of  $\Delta\rho^\sigma(r) = \lambda[\rho_{\text{CBM}}^\sigma(r) - \rho_{\text{VBM}}^\sigma(r)]$  in illumination compared to the original steady state, where  $\lambda$  means the illumination strength, and  $\rho_{\text{CBM}}^\sigma(r)$  and  $\rho_{\text{VBM}}^\sigma(r)$  are the partial charge density of the spin-polarized CBM and VBM states, respectively. With this in mind, we can modify the charge density from the initial neutral defect state by adding  $\Delta\rho^\sigma$  to mimic the steady state under the illumination as Fig. 1(b) shown. We take the host as the example and the whole calculation process is summarized as follows:

(1) The calculation is started with initial wave function and the eigenvalues include occupied and unoccupied. We can get the total charge density ( $\sum_i^N f_i^\sigma |\Psi_i^\sigma(r)|^2$ ), VBM charge density ( $|\Psi_{\text{VBM}}^\sigma(r)|^2$ ), and CBM charge density ( $|\Psi_{\text{CBM}}^\sigma(r)|^2$ ) for the perfect semiconductor. At the same time, we also get the charge-density difference  $\Delta\rho^\sigma = \lambda(|\Psi_{\text{CBM}}^\sigma(r)|^2 - |\Psi_{\text{VBM}}^\sigma(r)|^2)$ ,  $\lambda$  is the strength of illumination means the number of excited electrons.

(2) In order to induce the illumination to the supercell, the charge correction is applied to the total charge density in each iterate step,

$$\rho_T = \sum_i^N f_i^\sigma |\Psi_i^\sigma(r)|^2 + \Delta\rho^\sigma(r). \quad (\text{A1})$$

(3) The potentials are determined by the  $N$ -electron charge density with  $\Delta\rho^\sigma(r)$ , and the total energy  $E^{il}$  can be calculated. It is noted that the  $E^{il}$  only count the energies of the lowest states of  $N$  electrons. Here, we need to make a correction for the total energy to include the eigenvalue of CBM:  $E_{\text{corr}}^{il} = E^{il} + \lambda(\varepsilon_{\text{CBM}} - \varepsilon_{\text{VBM}})$ .

## APPENDIX B: CONCENTRATION OF CHARGED DEFECTS UNDER ILLUMINATION

It can be shown that the probabilities of electrons occupying the donor-defect level [ $f_D(E)$ ] and holes occupying the

acceptor level [ $f_A(E)$ ] are

$$f_D(E) = \frac{1}{1 + \frac{1}{g_D} \exp\left(\frac{E_D - E_F}{k_B T}\right)}, \quad (\text{B1})$$

$$f_A(E) = \frac{1}{1 + \frac{1}{g_A} \exp\left(\frac{E_F - E_A}{k_B T}\right)}, \quad (\text{B2})$$

where  $g_A$  and  $g_D$  are, respectively, the degeneracy factor related to possible structural configurations and electron occupations of acceptor and donor. Here, denoting the total concentration of donor defects as  $N_D$  and concentration of acceptor defects as  $N_A$ , we can get the following formulas.

The electron concentration on the donor and acceptor defects are

$$n_D^0 = f_D(E)N_D = \frac{N_D}{1 + \frac{1}{g_D} \exp\left(\frac{E_D - E_F}{k_B T}\right)}, \quad (\text{B3})$$

$$n_A^0 = f_A(E)N_A = \frac{N_A}{1 + \frac{1}{g_A} \exp\left(\frac{E_F - E_A}{k_B T}\right)}. \quad (\text{B4})$$

Then, the ionized donor and acceptor defect concentrations are

$$n_D^+ = (1 - f_D(E))N_D = \frac{1}{g_D} \exp\left(\frac{E_D - E_F}{k_B T}\right)n_D^0, \quad (\text{B5})$$

$$n_A^- = (1 - f_A(E))N_A = \frac{1}{g_A} \exp\left(\frac{E_F - E_A}{k_B T}\right)n_A^0. \quad (\text{B6})$$

Then, the concentration of charged defects can be expressed more generally as

$$N(\alpha, q) = \exp\left(\frac{q*(E_i^\alpha - E_F)}{k_B T}\right) N(\alpha, 0), \# \quad (\text{B7})$$

$$N(\alpha, 0) = g \exp\left(\frac{-\Delta H_f(\alpha, 0)}{k_B T}\right) N_{\text{site}}(\alpha), \# \quad (\text{B8})$$

where  $E_D$ ,  $E_A$ , and  $E_i^\alpha$  are the defect-transition level,  $N_{\text{site}}(\alpha)$  is the number of possible sites of defect  $\alpha$  in a supercell, and  $g$  is the degeneracy factor of the electron occupations.  $E_i$  is the defect-transition energy level.  $\Delta H_f(\alpha, 0)$  is the formation energy of defect  $\alpha$  at charge state 0. Under the equilibrium state with illumination, the occupation of defect states changes due to the increase in electron temperature.

### APPENDIX C: NATIVE DEFECT PROPERTIES IN MoS<sub>2</sub> MONOLAYER AND BULK

We use the norm-conserving pseudopotentials within the Perdew-Burke-Ernzerhof framework [44,45] to treat the valence electrons. For the Brillouin-zone integrals in the reciprocal space, the single  $\Gamma$  point is used for all calculations, which is accurate enough as the defect supercell is  $6 \times 6 \times 1$ . The kinetic energy cutoff of the plane-wave basis is 80 Ry and the total energy threshold for the convergence is  $10^{-8}$  Ry. All atoms are relaxed until the Hellman-Feynman forces on individual atoms are less than  $10^{-4}$  Ry/bohr.

We start the discussion of the results by calculating the formation energies and ionization energies of the candidate defects. Using the charge-correction method, we calculate the properties of both intrinsic defects  $V_S$ ,  $V_{\text{Mo}}$ ,  $\text{Mo}_i$ ,  $S_i$  and the impurity  $\text{Nb}_{\text{Mo}}$  in MoS<sub>2</sub> monolayer which have

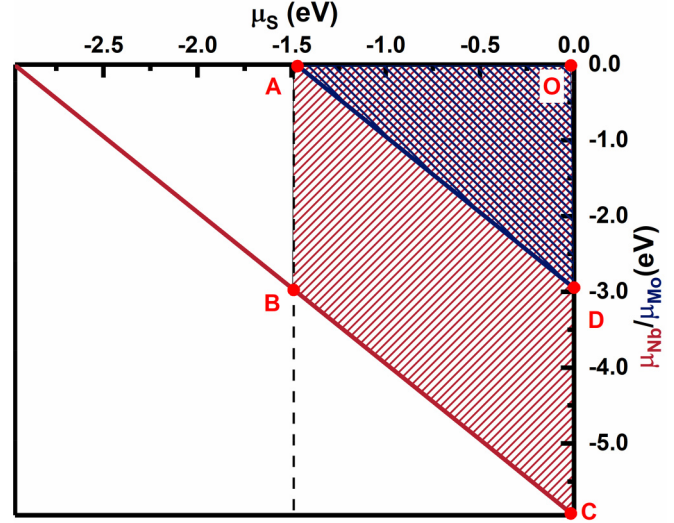


FIG. 6. Stable chemical potential range of MoS<sub>2</sub> and NbS<sub>2</sub> under thermal equilibrium growth condition. Area  $O-A-D$  represents chemical potential curve of stable formation of MoS<sub>2</sub> and  $O-A-B-C$  is stable for NbS<sub>2</sub>.

been reported in previous papers [31,32]. The chemical potentials  $\mu_{\text{Mo}}$ ,  $\mu_{\text{Nb}}$ , and  $\mu_S$  need to satisfy  $\mu_{\text{Mo}} + 2\mu_S = \Delta H_f(\text{MoS}_2) = -2.95$  eV and  $\mu_{\text{Nb}} + 2\mu_S = \Delta H_f(\text{NbS}_2) = -5.94$  eV to form stable MoS<sub>2</sub> and NbS<sub>2</sub>, where  $\Delta H_f(\text{MoS}_2)$  and  $\Delta H_f(\text{NbS}_2)$  are the formation enthalpy of MoS<sub>2</sub> and NbS<sub>2</sub> monolayer, respectively. To make sure MoS<sub>2</sub> monolayer stabilizes under equilibrium growth conditions, the atomic chemical potentials need to satisfy certain condition:  $\mu_{\text{Mo}} + 2\mu_S < \Delta H_f(\text{MoS}_2) = -2.95$  eV. Under this constraint, the chemical potentials of Mo and S that can stabilize MoS<sub>2</sub> are bound to a triangle in the two-dimensional ( $\mu_{\text{Mo}}$  and  $\mu_S$ ) space, as shown in Fig. 6. The chemical potentials of Mo and S are limited within 0.0 to  $-2.95$  eV and 0.0 to  $-1.475$  eV, respectively. Nb behaves as an acceptor in MoS<sub>2</sub>, and we doped it to realize  $p$ -type MoS<sub>2</sub>. So, the chemical potential of Nb-doped MoS<sub>2</sub> should satisfy  $\mu_{\text{Nb}} + 2\mu_S < \Delta H_f(\text{NbS}_2) = -5.94$  eV at the same time. As a result, the  $\mu_S$  would be fixed at  $-1.475$  eV at the Mo-rich condition ( $\mu_{\text{Mo}} = 0$  eV). At this time,  $\mu_{\text{Nb}}$  can be any value between 0.00 and  $-3.0$  eV. Considering the doping concentration, we set the  $\mu_{\text{Nb}} = -1$  eV.

The calculated energies of isolated native point defects, including monovacancy ( $V_S$ ,  $V_{\text{Mo}}$ ), interstitial ( $\text{Mo}_i$ ,  $S_i$ ), and impurity ( $\text{Nb}_{\text{Mo}}$ ), before and after illumination are shown in Fig. 2. Without illumination ( $\lambda = 0$ ), among all of the native defects,  $V_S$  has the lowest formation energy under Mo-rich conditions. The same as previous works [46],  $V_S$  acts as a deep electron trap center in MoS<sub>2</sub> monolayer because the  $\varepsilon(0/-1)$  and  $\varepsilon(0/-2)$  transition level is close to the CBM and occurs 1.26 and 1.32 eV above the VBM. Except  $V_S$ , the formation energies of other defects are relatively high, which means those defects are difficult to form under the Mo-rich condition. Niobium has been reported as an effective impurity to realize  $p$ -type doping in MoS<sub>2</sub> thin films [47]. Based on our calculation, we find  $\text{Nb}_{\text{Mo}}$  has a relative low formation energy, implying  $\text{Nb}_{\text{Mo}}$  can be formed with a high concentration.



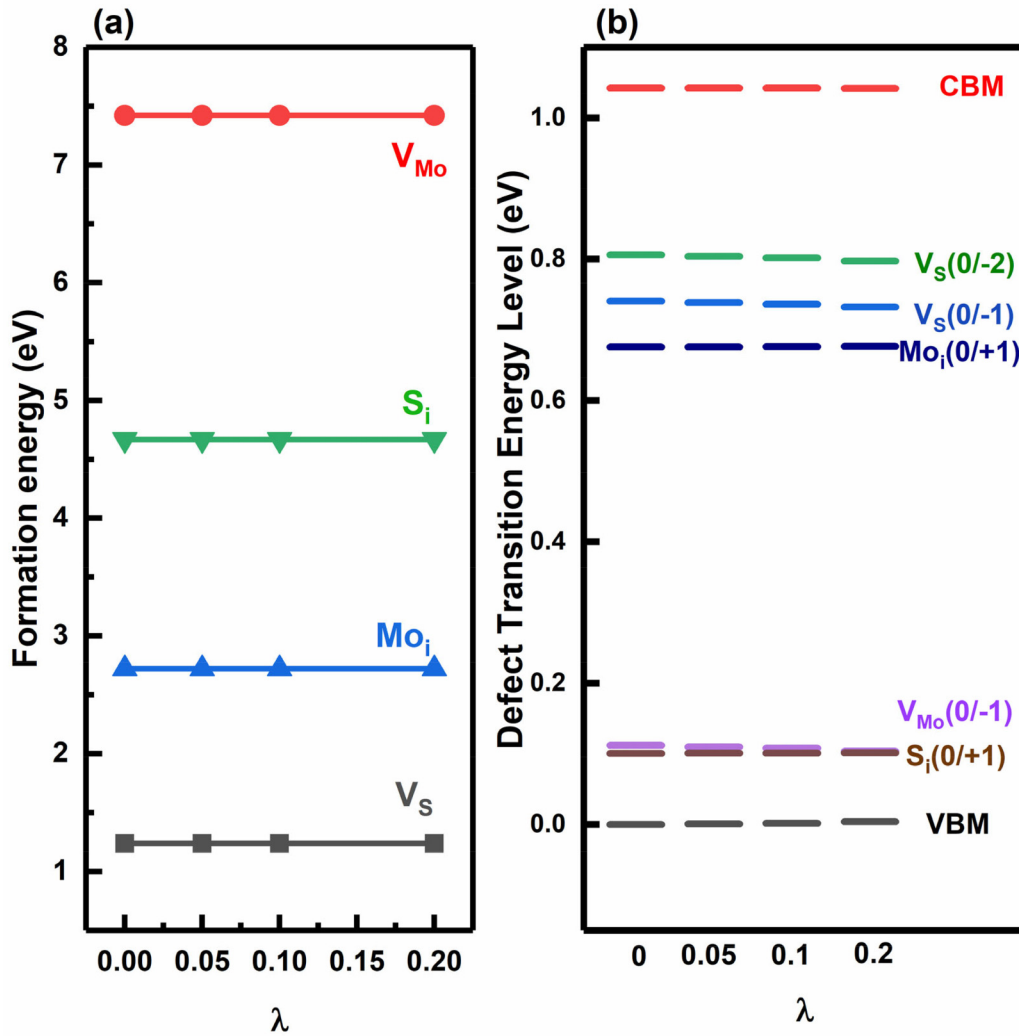


FIG. 7. Illumination effects on formation energies of neutral defects and defect-transition energy levels in MoS<sub>2</sub> bulk. (a) Formation energies of neutral defects and (b) defect-transition energy levels as functions of illumination strengths.  $\lambda$  represents number of excited electrons in supercell, and defect-transition levels are referenced to VBM without illumination.

Furthermore,  $Nb_{Mo}$  is a shallow acceptor and has significant contribution to conductivity in MoS<sub>2</sub> monolayer.

For MoS<sub>2</sub> bulk system, we adopt Mo-rich situation which is the same with monolayer. As shown in Fig. 7, the change of formation energy is less than 0.1 meV and that of defect-transition energy level is less than 1 meV. The reasons can be attributed to the delocalization of band-edge states, which do not have significant effects on localized properties such as formation and ionization of an isolated defect. Our results demonstrate that illumination effects on bulk structure are the same as two-dimensional semiconductors.

#### APPENDIX D: NONEQUILIBRIUM STEADY-STATE CONDITION

Under the nonequilibrium steady state, the generated and recombined number of carriers per unit area and per unit time must be equal. Assuming the photogeneration rate of electrons and holes is  $G$ , we get

$$G - R_{BB} - R_{Aug} - \sum_{\alpha, q} R_{SRH}(\alpha, q) = 0, \quad (D1)$$

where  $R_{BB}$ ,  $R_{Aug}$ , and  $R_{SRH}(\alpha, q)$  are the band-to-band, Auger, and defect-assisted Shockly-Read-Hall recombination rates, respectively. They can be given by

$$R_{BB} = B\gamma, \quad R_{Aug} = (A_n n + A_p p)\gamma, \quad (D2)$$

$$R_{SRH}(\alpha, q) = \frac{\gamma * N^{il}(\alpha, q)}{(n + n_t)/c_p + (p + p_t)/c_n}, \quad (D3)$$

in which  $\gamma = (np - n_i^2)$ ,  $c_n = \sigma_n v_{th}$ ,  $c_p = \sigma_p v_{th}$ , and  $v_{th}^2 = 3kT/m^*$ .  $n_t$  and  $p_t$  are the electron and hole concentrations when the Fermi level coincides with the trap level.  $B$ ,  $A_n(A_p)$ ,  $c_n(c_p)$ ,  $\sigma_n(\sigma_p)$ , and  $v_{th}$  denote the rate of radiative capture probability, Auger coefficients of electrons (holes), capture cross section of electrons (holes), and average thermal velocity of electrons or holes, respectively. These quantities are difficult to obtain either experimentally or theoretically.

#### APPENDIX E: HOW TO DETERMINE THE $N_V$ AND $N_C$ UNDER ILLUMINATION

First, as long as there is no magnitude change for  $N_V$  ( $N_C$ ), whether  $T$  or  $T'$  is used to obtain the  $N_V$  ( $N_C$ ) does not have

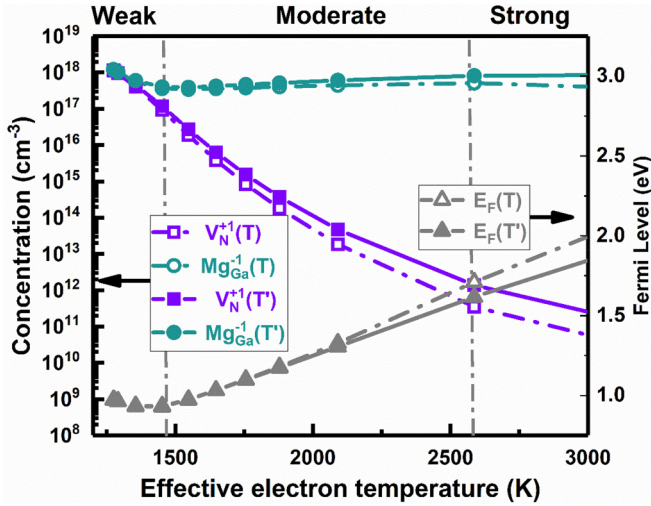


FIG. 8. Concentrations of charged defects and effective Fermi level as functions of illumination intensities when GaN is grown at 1275 K. Dashed and solid lines represent results calculated by using  $T$  and  $T'$ , respectively.

a significant influence on the result. In Fig. 8, we compare the results calculated by using  $T$  and  $T'$ , respectively, to obtain the  $N_V$  ( $N_C$ ) for GaN. As can be seen, there are only some slight differences when the illumination intensity is strong. In practice, because the illumination should have some effect on the  $N_V$  ( $N_C$ ), we think  $T'$  is a better choice than  $T$  to calculate  $N_V$  ( $N_C$ ).

APPENDIX F: CALCULATION DETAILS IN GaN:Mg

We use the projector augmented wave (PAW) method and the Heyd-Scuseria-Ernzerhof hybrid density functional [48] as implemented in VASP package [44,45] to treat the valence

electrons. We set the Hartree-Fock exchange mixing parameter  $\alpha$  to 0.31. For the Brillouin zone integrals in the reciprocal space, the single  $\Gamma$  point is used for all calculations, which is accurate enough as the defect supercell is  $3 \times 4 \times 2$  with 96 atoms. The kinetic energy cutoff of the plane wave basis is 600 eV and the total energy threshold for the convergence is  $10^{-8}$  eV. All atoms are relaxed until the Hellman-Feynman forces on individual atoms are less than  $10^{-2}$  eV/Å.

In our theory, both the effective electron temperature ( $T'$ ) and the concentration of photo-induced carriers ( $\Delta n$ ) can be used to describe the intensity of illumination and are equivalent to each other based on the following equations:

$$n' = N_C(T') \exp\left(-\frac{E_C - E'_F}{k_B T'}\right), \tag{F1}$$

$$p' = N_V(T') \exp\left(-\frac{E'_F - E_V}{k_B T'}\right), \tag{F2}$$

$$\Delta n = n' - n, \tag{F3}$$

In any case, we can use  $T'$  or  $n'p'$  ( $\Delta n$ ,  $\Delta p$ ) to represent the illumination intensities without considering complicated parameters like recombination rates. Compared to the  $T'$ ,  $\Delta n$  is more direct in comparing with experimental values. As a result, we used  $\Delta n$  to represent the illumination intensity in the manuscript and didn't mention the values of  $T'$ . Here, we can also use  $T'$  to represent the illumination strength (see Fig. 10). As can be seen that, the results are consistent with each other.

APPENDIX G: ILLUMINATION EFFECTS ON CdTe:Sb

CdTe is a semiconductor of great importance to many devices, including scintillators to detect gamma rays, electrical-optical modulators, and thin-film solar cells. Device modeling

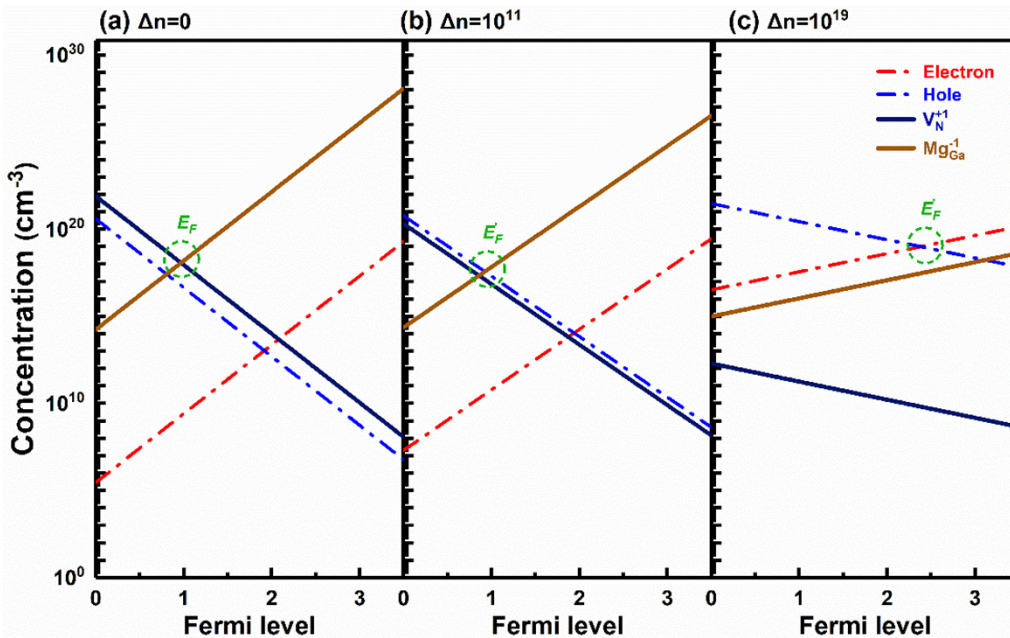


FIG. 9. Concentrations of charged defects and carriers as functions of Fermi level under different illumination conditions. (a)–(c) Concentrations under no, weak, and strong illuminations, respectively. Solid lines are for defects and dashed lines are for band-edge carriers.

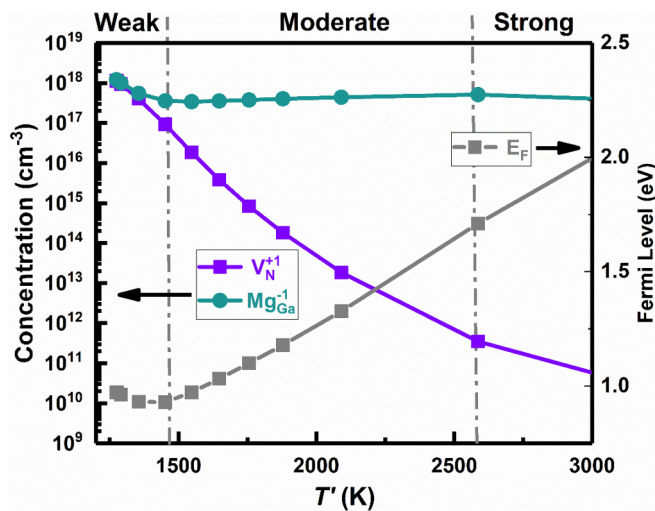


FIG. 10. Concentrations of charged defects and effective Fermi level as functions of illumination strengths  $T'$  when GaN is grown at 1275 K.

simulations suggest that by increasing the hole concentration in the CdTe absorber from  $10^{14} \text{ cm}^{-3}$  (for typical undoped CdTe films) to  $10^{16} \text{ cm}^{-3}$  would lead to photovoltaic efficiency reaching 25% [49]. Adding group-V impurities, such as P, As, and Sb, would constitute the most straightforward way of controllably increasing the hole concentration [7,10,50,51]. In order to achieve a higher hole concentration, the photoassisted molecular-beam epitaxy growth technique

is widely used in the doping process of  $p$ -type CdTe [10,50]. Here, we take Sb-doped CdTe as an example and choose the Te-poor condition.

The calculations are conducted with the projector augmented-wave method and the HSE06 hybrid density functional [48] as implemented in the VASP package. We set the Hartree-Fock exchange mixing parameter  $\alpha$  to 0.25 and a cutoff energy to 600 eV for the plane-wave basis set. We construct a 64-atom supercell for the defect system. The calculated lattice constant of pure CdTe is 6.56 Å with a band gap of 1.49 eV, in good agreement with previous works [52]. A common experimental growth temperature of 500 K and electron and hole effective masses of  $0.095m_0$  and  $0.84m_0$ , respectively, are applied [50,53]. Based on our calculations,  $\text{Sb}_{\text{Te}}$  has a  $(0/-1)$  transition energy level around 0.13 eV above the VBM, which is in good agreement with previous reported data [7,43,51,54].

The calculated defect-formation energies as functions of the Fermi level under the Ga-rich conditions are shown in Fig. 11. The lines for band-edge defects are also given at  $T = 500 \text{ K}$ , which is a typical experimental growth temperature. When illumination is applied, the effective temperature of electrons starts to increase from  $T$  to  $T'$ . Note that given illumination strengths and thus  $T'$ , defect concentrations, carrier densities, and the  $E'_F$  can be obtained by self-consistently solving Eqs. (4)–(9) in the main text at a given growth temperature  $T$ . In the following, we use  $\Delta n = n' - n_0$  to denote illumination strengths, where  $n'$  and  $n_0$  are the electron densities at electron temperatures of  $T'$  and  $T$  (here,  $T = 500 \text{ K}$ ), respectively.

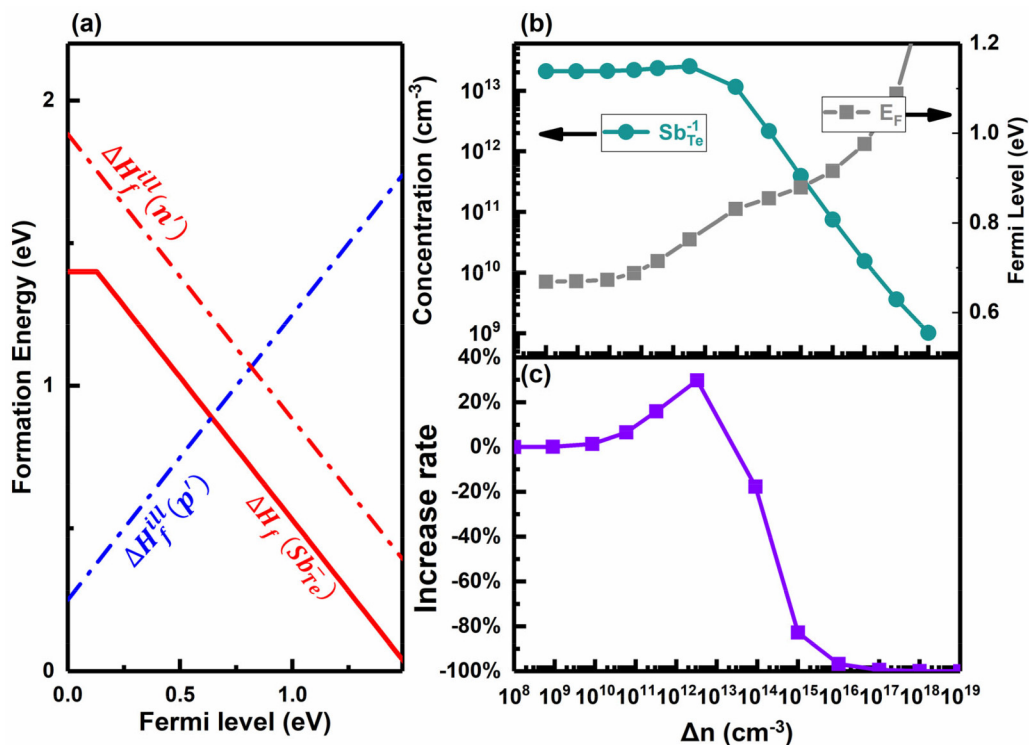


FIG. 11. Illumination effects on defect properties of Sb-doped CdTe. (a) Defect-formation energies as functions of Fermi level in Sb-doped CdTe. (b) Concentrations of charged defects and effective Fermi level as functions of illumination strengths when CdTe is grown at 500 K. (c) Increase rate of Sb concentration, set concentration without illumination as reference.

Without illumination, the Fermi level is pinned at point 0.46 eV; the  $E'_F$  would be mainly determined by the concentration of  $\text{Sb}_{\text{Te}}^-$  and holes. When illumination is applied, the  $E'_F$  will move to the middle of the gap. According to Eq. (6) in the main text, for negatively charged defect  $\text{Sb}_{\text{Te}}^-$ , because  $q(E'_i - E'_F)$  increases faster than  $T'$ , its concentration

slightly increases according to our calculations [see Fig. S6(b)]. Nevertheless, the doping concentration of Sb in CdTe was significantly increased [see Fig. 11(c)], which is in good agreement with a previous experimentally reported 20% concentration increase [10].

- 
- [1] H. Fang, M. Tosun, G. Seol, T. C. Chang, K. Takei, J. Guo, and A. Javey, Degenerate n-doping of few-layer transition metal dichalcogenides by potassium, *Nano Lett.* **13**, 1991 (2013).
- [2] H.-J. Chuang, B. Chamlagain, M. Koehler, M. M. Perera, J. Yan, D. Mandrus, D. Tománek, and Z. Zhou, Low-resistance 2D/2D Ohmic contacts: A universal approach to high-performance  $\text{WSe}_2$ ,  $\text{MoS}_2$ , and  $\text{MoSe}_2$  transistors, *Nano Lett.* **16**, 1896 (2016).
- [3] Y. Xu, C. Cheng, S. Du, J. Yang, B. Yu, J. Luo, W. Yin, E. Li, S. Dong, P. Ye, and X. Duan, Contacts between two- and three-dimensional materials: Ohmic, Schottky, and p-n heterojunctions, *ACS Nano* **10**, 4895 (2016).
- [4] S. Wang, M. Huang, Y.-N. Wu, W. Chu, J. Zhao, A. Walsh, X.-G. Gong, S.-H. Wei, and S. Chen, Effective lifetime of non-equilibrium carriers in semiconductors from non-adiabatic molecular dynamics simulations, *Nat. Comput. Sci.* **2**, 486 (2022).
- [5] L. Cheng, C. Zhang, and Y. Liu, Why two-dimensional semiconductors generally have low electron mobility, *Phys. Rev. Lett.* **125**, 177701 (2020).
- [6] G.-J. Zhu, Y.-G. Xu, X.-G. Gong, J.-H. Yang, and B. I. Yakobson, Dimensionality-inhibited chemical doping in two-dimensional semiconductors: The phosphorene and  $\text{MoS}_2$  from charge-correction method, *Nano Lett.* **21**, 6711 (2021).
- [7] I. Chatratin, B. Dou, S.-H. Wei, and A. Janotti, Doping limits of phosphorus, arsenic, and antimony in CdTe, *J. Phys. Chem. Lett.* **14**, 273 (2023).
- [8] X. Li, B. Zhang, H. Zhu, X. Dong, X. Xia, Y. Cui, K. Huang, and G. Du, Properties of ZnO thin films grown on Si substrates by photo-assisted MOCVD, *Appl. Surf. Sci.* **254**, 2081 (2008).
- [9] X. Cai, J.-W. Luo, S.-S. Li, S.-H. Wei, and H.-X. Deng, Overcoming the doping limit in semiconductors via illumination, *Phys. Rev. B* **106**, 214102 (2022).
- [10] J. D. Benson, D. Rajavel, B. K. Wagner, R. Benz, and C. J. Summers, Properties of undoped and Sb-doped CdTe surfaces prepared by conventional and photo-assisted molecular beam epitaxy, *J. Cryst. Growth* **95**, 543 (1989).
- [11] H. Tsai, R. Asadpour, J.-C. Blancon, C. C. Stoumpos, O. Durand, J. W. Strzalka, B. Chen, R. Verduzco, P. M. Ajayan, S. Tretiak, J. Even, M. A. Alam, M. G. Kanatzidis, W. Nie, and A. D. Mohite, Light-induced lattice expansion leads to high-efficiency perovskite solar cells, *Science* **360**, 67 (2018).
- [12] E. T. Hoke, D. J. Slotcavage, E. R. Dohner, A. R. Bowring, H. I. Karunadasa, and M. D. McGehee, Reversible photo-induced trap formation in mixed-halide hybrid perovskites for photovoltaics, *Chem. Sci.* **6**, 613 (2015).
- [13] Z. Bryan, I. Bryan, B. E. Gaddy, P. Reddy, L. Hussey, M. Bobea, W. Guo, M. Hoffmann, R. Kirste, J. Tweedie, M. Gerhold, D. L. Irving, Z. Sitar, and R. Collazo, Fermi level control of compensating point defects during metalorganic chemical vapor deposition growth of Si-doped AlGaN, *Appl. Phys. Lett.* **105**, 222101 (2014).
- [14] K. Alberi and M. A. Scarpulla, Effects of excess carriers on charged defect concentrations in wide bandgap semiconductors, *J. Appl. Phys.* **123**, 185702 (2018).
- [15] K. Alberi and M. A. Scarpulla, Suppression of compensating native defect formation during semiconductor processing via excess carriers, *Sci. Rep.* **6**, 27954 (2016).
- [16] P. Reddy, M. P. Hoffmann, F. Kaess, Z. Bryan, I. Bryan, M. Bobea, A. Klump, J. Tweedie, R. Kirste, S. Mita, M. Gerhold, R. Collazo, and Z. Sitar, Point defect reduction in wide bandgap semiconductors by defect quasi Fermi level control, *J. Appl. Phys.* **120**, 185704 (2016).
- [17] P. Reddy, F. Kaess, J. Tweedie, R. Kirste, S. Mita, R. Collazo, and Z. Sitar, Defect quasi Fermi level control-based CN reduction in GaN: Evidence for the role of minority carriers, *Appl. Phys. Lett.* **111**, 152101 (2017).
- [18] B. Peng, D. Bennett, I. Bravić, and B. Monserrat, Tunable photostriction of halide perovskites through energy dependent photoexcitation, *Phys. Rev. Mater.* **6**, L082401 (2022).
- [19] G.-J. Zhu, J.-H. Yang, and X.-G. Gong, Self-consistently determining structures of charged defects and defect ionization energies in low-dimensional semiconductors, *Phys. Rev. B* **102**, 035202 (2020).
- [20] H.-X. Deng and S.-H. Wei, Comment on “fundamental resolution of difficulties in the theory of charged point defects in semiconductors”, *Phys. Rev. Lett.* **120**, 039601 (2018).
- [21] P. Giannozzi, S. Baroni, N. Bonini, M. Calandra, R. Car, C. Cavazzoni, D. Ceresoli, G. L. Chiarotti, M. Cococcioni, I. Dabo, A. Dal Corso, S. de Gironcoli, S. Fabris, G. Fratesi, R. Gebauer, U. Gerstmann, C. Gougoussis, A. Kokalj, M. Lazzeri, L. Martin-Samos, N. Marzari, F. Mauri, R. Mazzarello, S. Paolini, A. Pasquarello, L. Paulatto, C. Sbraccia, S. Scandolo, G. Sclauzero, A. P. Seitsonen, A. Smogunov, P. Umari, and R. M. Wentzcovitch, QUANTUM ESPRESSO: A modular and open-source software project for quantum simulations of materials, *J. Phys.: Condens. Matter* **21**, 395502 (2009).
- [22] S. Lany and A. Zunger, Accurate prediction of defect properties in density functional supercell calculations, *Modell. Simul. Mater. Sci. Eng.* **17**, 084002 (2009).
- [23] C. Freysoldt, J. Neugebauer, and C. G. Van de Walle, Fully *ab initio* finite-size corrections for charged-defect supercell calculations, *Phys. Rev. Lett.* **102**, 016402 (2009).
- [24] M. Leslie and N. J. Gillan, The energy and elastic dipole tensor of defects in ionic crystals calculated by the supercell method, *J. Phys. C: Solid State Phys.* **18**, 973 (1985).
- [25] C. Freysoldt, J. Neugebauer, A. M. Z. Tan, and R. G. Hennig, Limitations of empirical supercell extrapolation for calculations of point defects in bulk, at surfaces, and in two-dimensional materials, *Phys. Rev. B* **105**, 014103 (2022).

- [26] M. Cavallini and D. Gentili, Atomic vacancies in transition metal dichalcogenides: Properties, fabrication, and limits, *ChemPlusChem* **87**, e202100562 (2022).
- [27] A. Ebnonnasir, B. Narayanan, S. Kodambaka, and C. V. Ciobanu, Tunable MoS<sub>2</sub> bandgap in MoS<sub>2</sub>-graphene heterostructures, *Appl. Phys. Lett.* **105**, 031603 (2014).
- [28] M. P. K. Sahoo, J. Wang, Y. Zhang, T. Shimada, and T. Kitamura, Modulation of gas adsorption and magnetic properties of monolayer-MoS<sub>2</sub> by antisite defect and strain, *J. Phys. Chem. C* **120**, 14113 (2016).
- [29] D. Y. Qiu, F. H. da Jornada, and S. G. Louie, Optical spectrum of MoS<sub>2</sub>: Many-body effects and diversity of exciton states, *Phys. Rev. Lett.* **111**, 216805 (2013).
- [30] F. Li, B. Xu, W. Yang, Z. Qi, C. Ma, Y. Wang, X. Zhang, Z. Luo, D. Liang, D. Li, Z. Li, and A. Pan, High-performance optoelectronic devices based on van der Waals vertical MoS<sub>2</sub>/MoSe<sub>2</sub> heterostructures, *Nano Res.* **13**, 1053 (2020).
- [31] H.-P. Komsa and A. V. Krasheninnikov, Native defects in bulk and monolayer MoS<sub>2</sub> from first principles, *Phys. Rev. B* **91**, 125304 (2015).
- [32] J.-Y. Noh, H. Kim, and Y.-S. Kim, Stability and electronic structures of native defects in single-layer MoS<sub>2</sub>, *Phys. Rev. B* **89**, 205417 (2014).
- [33] J.-H. Yang, W.-J. Yin, J.-S. Park, and S.-H. Wei, Self-regulation of charged defect compensation and formation energy pinning in semiconductors, *Sci. Rep.* **5**, 16977 (2015).
- [34] J. Buckeridge, C. R. A. Catlow, D. O. Scanlon, T. W. Keal, P. Sherwood, M. Miskufova, A. Walsh, S. M. Woodley, and A. A. Sokol, Determination of the nitrogen vacancy as a shallow compensating center in GaN doped with divalent metals, *Phys. Rev. Lett.* **114**, 016405 (2015).
- [35] A. Bhattacharyya, W. Li, J. Cabalu, T. D. Moustakas, D. J. Smith, and R. L. Hergiv, Efficient p-type doping of GaN films by plasma-assisted molecular beam epitaxy, *Appl. Phys. Lett.* **85**, 4956 (2004).
- [36] Z. Bryan, M. Hoffmann, J. Tweedie, R. Kirste, G. Callsen, I. Bryan, A. Rice, M. Bobea, S. Mita, J. Xie, Z. Sitar, and R. Collazo, Fermi level control of point defects during growth of Mg-doped GaN, *J. Electron. Mater.* **42**, 815 (2013).
- [37] C. E. Sanders, D. A. Beaton, R. C. Reedy, and K. Alberi, Fermi energy tuning with light to control doping profiles during epitaxy, *Appl. Phys. Lett.* **106**, 182105 (2015).
- [38] K. Alberi and M. A. Scarpulla, Photoassisted physical vapor epitaxial growth of semiconductors: A review of light-induced modifications to growth processes, *J Phys D: Appl Phys* **51**, 023001 (2018).
- [39] J. L. Lyons and C. G. Van de Walle, Computationally predicted energies and properties of defects in GaN, *npj Comput. Mater.* **3**, 12 (2017).
- [40] U. Kaufmann, P. Schlotter, H. Obloh, K. Köhler, and M. Maier, Hole conductivity and compensation in epitaxial GaN:Mg layers, *Phys. Rev. B* **62**, 10867 (2000).
- [41] A. Klump, M. P. Hoffmann, F. Kaess, J. Tweedie, P. Reddy, R. Kirste, Z. Sitar, and R. Collazo, Control of passivation and compensation in Mg-doped GaN by defect quasi Fermi level control, *J. Appl. Phys.* **127**, 045702 (2020).
- [42] F. Kaess, P. Reddy, D. Alden, A. Klump, L. H. Hernandez-Balderrama, A. Franke, R. Kirste, A. Hoffmann, R. Collazo, and Z. Sitar, The effect of illumination power density on carbon defect configuration in silicon doped GaN, *J. Appl. Phys.* **120**, 235705 (2016).
- [43] J.-H. Yang, J.-S. Park, J. Kang, W. Metzger, T. Barnes, and S.-H. Wei, Tuning the Fermi level beyond the equilibrium doping limit through quenching: The case of CdTe, *Phys. Rev. B* **90**, 245202 (2014).
- [44] G. Kresse and J. Furthmüller, Efficient iterative schemes for ab initio total-energy calculations using a plane-wave basis set, *Phys. Rev. B* **54**, 11169 (1996).
- [45] J. P. Perdew and M. Levy, Physical content of the exact Kohn-Sham Orbital Energies: Band gaps and derivative discontinuities, *Phys. Rev. Lett.* **51**, 1884 (1983).
- [46] A. Singh and A. K. Singh, Origin of *n*-type conductivity of monolayer MoS<sub>2</sub>, *Phys. Rev. B* **99**, 121201(R) (2019).
- [47] M. R. Laskar, D. N. Nath, L. Ma, E. W. Lee, C. H. Lee, T. Kent, Z. Yang, R. Mishra, M. A. Roldan, J.-C. Idrobo, S. T. Pantelides, S. J. Pennycook, R. C. Myers, Y. Wu, and S. Rajan, p-type doping of MoS<sub>2</sub> thin films using Nb, *Appl. Phys. Lett.* **104**, 092104 (2014).
- [48] J. Heyd, G. E. Scuseria, and M. Ernzerhof, Hybrid functionals based on a screened Coulomb potential, *J. Phys. Chem.* **118**, 8207 (2003).
- [49] A. Kanevce, M. O. Reese, T. M. Barnes, S. A. Jensen, and W. K. Metzger, The roles of carrier concentration and interface, bulk, and grain-boundary recombination for 25% efficient CdTe solar cells, *J. Appl. Phys.* **121**, 214506 (2017).
- [50] R. L. Harper, S. Hwang, N. C. Giles, J. F. Schetzina, D. L. Dreifus, and T. H. Myers, Arsenic-doped CdTe epilayers grown by photoassisted molecular beam epitaxy, *Appl. Phys. Lett.* **54**, 170 (1989).
- [51] E. Colegrove, J. H. Yang, S. P. Harvey, M. R. Young, J. M. Burst, J. N. Duenow, D. S. Albin, S. H. Wei, and W. K. Metzger, Experimental and theoretical comparison of Sb, As, and P diffusion mechanisms and doping in CdTe, *J Phys D: Appl Phys* **51**, 075102 (2018).
- [52] J.-H. Yang, L. Shi, L.-W. Wang, and S.-H. Wei, Non-radiative carrier recombination enhanced by two-level process: A first-principles study, *Sci. Rep.* **6**, 21712 (2016).
- [53] J. Ma, S.-H. Wei, T. A. Gessert, and K. K. Chin, Carrier density and compensation in semiconductors with multiple dopants and multiple transition energy levels: Case of Cu impurities in CdTe, *Phys. Rev. B* **83**, 245207 (2011).
- [54] B. Dou, Q. Sun, and S.-H. Wei, Optimization of doping CdTe with group-V elements: A first-principles study, *Phys. Rev. Appl.* **15**, 054045 (2021).